Laboratory measurements of HDO/H_2O isotopic fractionation during ice deposition in simulated cirrus clouds

Kara D. Lamb[a,1], Benjamin W. Clouser[a], Maximilien Bolot[b,2], Laszlo Sarkozy[b], Volker Ebert[c], Harald Saathoff[d], Ottmar Möhler[d], and Elisabeth J. Moyer[b,3]

[a]Department of Physics, University of Chicago, Chicago, IL 60637; [b]Department of the Geophysical Sciences, University of Chicago, Chicago, IL 60637; [c]Physikalisch-Technische Bundesanstalt, 38116 Braunschweig, Germany; and [d]Institute for Meteorology and Climate Research, Karlsruhe Institute of Technology, 76021 Karlsruhe, Germany

Edited by Mark H. Thiemens, University of California, San Diego, La Jolla, CA, and approved April 5, 2017 (received for review November 5, 2016)

The stable isotopologues of water have been used in atmospheric and climate studies for over 50 years, because their strong temperature-dependent preferential condensation makes them useful diagnostics of the hydrological cycle. However, the degree of preferential condensation between vapor and ice has never been directly measured at temperatures below 233 K (−40 °C), conditions necessary to form cirrus clouds in the Earth's atmosphere, routinely observed in polar regions, and typical for the near-surface atmospheric layers of Mars. Models generally assume an extrapolation from the warmer experiments of Merlivat and Nief [Merlivat L, Nief G (1967) *Tellus* 19:122–127]. Nonequilibrium kinetic effects that should alter preferential partitioning have also not been well characterized experimentally. We present here direct measurements of HDO/H_2O equilibrium fractionation between vapor and ice (α_{eq}) at cirrus-relevant temperatures, using in situ spectroscopic measurements of the evolving isotopic composition of water vapor during cirrus formation experiments in a cloud chamber. We rule out the recent proposed upward modification of α_{eq}, and find values slightly lower than Merlivat and Nief. These experiments also allow us to make a quantitative validation of the kinetic modification expected to occur in supersaturated conditions in the ice–vapor system. In a subset of diffusion-limited experiments, we show that kinetic isotope effects are indeed consistent with published models, including allowing for small surface effects. These results are fundamental for inferring processes on Earth and other planets from water isotopic measurements. They also demonstrate the utility of dynamic in situ experiments for studying fractionation in geochemical systems.

isotopic fractionation | water vapor | cirrus clouds | ice deposition | diffusivity ratio

Accurate values of the vapor–ice isotopic fractionation factor are needed for many studies in paleoclimate, atmospheric science, or planetary science that use HDO/H_2O measurements as tracers: for paleotemperature or paleoaltimetry reconstructions with process-based models (1), for characterizing the hydrological cycle (2–4), for diagnosing convective transport of water to the tropical tropopause layer (TTL) (5–9), and for understanding the sources of water and the history of hydrogen escape on Mars (10, 11). In Earth's atmosphere, HDO has been measured by in situ balloon and aircraft instruments (6, 12), by nadir-sounding satellite instruments (13, 14), and by limb sounders that look at the edge of Earth's atmosphere and produce high-vertical-resolution profiles (15–17). The ExoMars mission, launched in 2016, will measure similar profiles on Mars (18). To date, water isotopologues have been introduced into at least 10 general circulation models of Earth (e.g., refs. 19–21) and one of Mars (10). The science conclusions drawn from comparing model output to isotopic measurements depend sensitively on the models' assumed value for isotopic fractionation. For the HDO/H_2O system, all use extrapolations of α_{eq} from the measurements of Merlivat and Nief (22) at temperatures warmer than the regime for cirrus formation. (We denote the expression for the temperature dependence in ref. 22 as M67.)

Measuring α_{eq} at cold temperatures is difficult largely because water vapor pressure becomes so small: in the cold uppermost troposphere, mixing ratios of H_2O can be a few parts per million, and those of HDO can be a few parts per billion. However, equilibrium fractionation becomes very large in these conditions, in part because the effect rises as $\sim 1/T^2$. The temperature dependence is typically assumed as

$$\alpha_{eq}(T) = \exp\left(a_0 + \frac{a_1}{T^2}\right), \quad [1]$$

the high-temperature limit for fractionation during gas condensation (23). Equilibrium fractionation in water is also particularly strong for deuterium substitution, because the effect scales to first order with the difference of the inverse of the isotopic masses (e.g., refs. 24 and 25).

In M67 (22), extrapolated to 190 K, α_{eq} exceeds 1.4 ($> 40\%$ HDO enhancement in ice), among the largest single-substitution

Significance

The preferential deposition of heavy water (HDO or $H_2^{18}O$) as ice is a fundamental tracer in the geosciences, used for understanding paleoclimate and water cycling, but the basic physical chemistry is not well measured. We describe here measurements of the preferential fractionation of HDO vs. H_2O at the cold temperatures relevant to cirrus clouds on Earth and snow on Mars. We also provide a quantitative demonstration of kinetic isotope effects in nonequilibrium conditions, and show how targeted dynamic experiments can be used to understand processes at ice surfaces.

Author contributions: K.D.L., M.B., and E.J.M. led the fractionation analysis; E.J.M. directed the construction and operation of ChiWIS; L.S. led the design of ChiWIS; K.D.L., B.W.C., and L.S. built and operated ChiWIS; K.D.L., B.W.C., and L.S. analyzed raw ChiWIS data to produce isotopic measurements; H.S. provided and operated multipass optics; H.S. and O.M. operated AIDA during the IsoCloud campaign; H.S. and O.M. provided and interpreted AIDA instrument data; V.E. provided SP-APicT and APeT data; and K.D.L., M.B., and E.J.M. wrote the paper.

The authors declare no conflict of interest.

This article is a PNAS Direct Submission.

Data deposition: The IsoCloud datasets and isotopic model can be found at https://publish.globus.org/jspui/handle/11466/247.

[1]Present address: Chemical Sciences Division, Earth System Research Laboratory, National Oceanic and Atmospheric Administration, Boulder, CO 80305.

[2]Present address: Program in Atmospheric and Oceanic Sciences, Princeton University, Princeton, NJ 08540.

[3]To whom correspondence should be addressed. Email: moyer@uchicago.edu.

This article contains supporting information online at www.pnas.org/lookup/suppl/doi:10.1073/pnas.1618374114/-/DCSupplemental.

vapor pressure isotope effects seen in natural systems. In 2013, Ellehøj et al. (26) reported measurements implying still stronger fractionation, with α_{eq} nearly 1.6 when extrapolated to 190 K, i.e., preferential partitioning α_{eq}-1 nearly 50% higher than implied by M67 (22). (We denote the expression for the temperature dependence in ref. 26 as E13; see *SI Appendix*, Table S1 for all previous estimates.) That difference would significantly alter interpretations of water isotopic measurements.

In many real-world conditions, kinetic effects during ice deposition can modify isotopic fractionation from the equilibrium case. Jouzel and Merlivat (27) explained nonequilibrium isotopic signatures in polar snow as the result of reduced effective fractionation when ice grows in diffusion-limited (and hence supersaturated) conditions, reasoning that preferential uptake should isotopically lighten the near-field vapor around growing ice crystals, with the effect amplified by the lower diffusivity of the heavier isotopologues. These diffusive effects are important for rain as well as snow, because most precipitation originates in mixed-phase (ice and liquid water) clouds, and can therefore alter "deuterium excess" in rainwater, a metric of nonequilibrium conditions that is often interpreted as reflecting only the initial evaporation of water (28). Despite the importance of kinetic effects during ice deposition, they are poorly characterized by experimental studies.

In the framework of Jouzel and Merlivat (27), the kinetic modification factor α_k can be written in terms of properties of the bulk gas,

$$\alpha_k = \frac{S_i}{\alpha_{eq} \cdot \mathrm{d}\,(S_i - 1) + 1}, \qquad [2]$$

where S_i is the supersaturation over ice and d (following the notation of ref. 29) is the isotopic ratio of diffusivities of water molecules in air. (That is, $\mathrm{d} = D_v/D'_v$, where D_v and D'_v are the molecular diffusivities of H_2O and HDO, respectively.) The effective isotopic fractionation is then $\alpha_{eff} = \alpha_{eq} \cdot \alpha_k$. The modification can be large at high supersaturations and cold temperatures, e.g., when ice nucleates homogeneously within aqueous sulfate aerosols in the upper troposphere ($S_i = 1.5$, T = 190 K). For ice growth occurring at these conditions, the preferential partitioning would be reduced by over 55% ($\alpha_{eq} = 1.43$, but $\alpha_{eff} = 1.24$) even conservatively using one of the lowest published estimates of d, that from Cappa et al. (ref. 30, d = 1.0164). The diffusive model of Eq. **2** is widely used but poorly validated. Kinetic effects during ice growth have been explored in three prior experimental studies (27, 31, 32). Although these provided qualitative support, relating supersaturated conditions to reduced fractionation or gradients in vapor isotopic composition, no experiments produced quantitative agreement with Eq. **2**.

Recent theoretical studies have proposed extending the diffusive model to include surface processes at the vapor–ice interface, which may become important when ice crystals are small (of order microns). In these conditions, surface impedance becomes comparable to vapor impedance, and any difference in deposition coefficients between isotopologues would contribute to kinetic isotope effects (29, 33). (The deposition coefficient quantifies the probability that a molecule incident on a growing ice crystal will be incorporated into the crystal lattice. Again following ref. 29, we define its isotopic ratio as $\mathrm{x} = \beta/\beta'$, where β and β' are the deposition coefficients for H_2O and HDO, respectively.) The deposition coefficient ratio has never been measured, but suggested plausible values of x = 0.8 to 1.2 would, in our example of upper tropospheric cirrus formation, further alter preferential partitioning by an additional 7 to 9%. Previous experimental studies of kinetic fractionation (27, 31, 32) were not sensitive to surface processes, because all involved large dendritic crystals in a regime where growth is not limited by surface effects (e.g., refs. 29, 34, and 35).

IsoCloud Campaigns

To investigate both equilibrium and kinetic isotopic effects at low temperatures, we carried out a series of experiments at the Aerosol Interactions and Dynamics in the Atmosphere (AIDA) cloud chamber during the 2012–2013 IsoCloud (Isotopic fractionation in Clouds) campaign. AIDA is a mature facility that has been widely used for studies of ice nucleation and cirrus formation (e.g., refs. 36–38). In the IsoCloud experiments, we determine isotopic fractionation not from static conditions as in previous studies but by measuring the evolving concentrations of HDO and H_2O vapor as ice forms. These experiments more closely replicate the conditions of ice formation in the atmosphere. Results reported here are derived from a new in situ tunable diode laser absorption instrument measuring HDO and H_2O (the Chicago Water Isotope Spectrometer, ChiWIS) and from AIDA instruments measuring total water, water vapor, ice crystal number density, temperature, and pressure (Fig. 1).

AIDA experiments produce rapid cooling inside the cloud chamber by pumping and adiabatic expansion, causing nucleation and growth of ice particles in situ. In a typical experiment (Fig. 2), cooling drives supersaturation above the threshold for ice nucleation within a minute of the onset of pumping. ($S_i \approx 1$ to 1.2 for heterogeneous and 1.4 to 1.6 for homogeneous nucleation.) As ice grows, the isotopic ratio of chamber water vapor lightens as the heavier isotopologues preferentially condense. For a typical cooling of 5 K to 9 K, water vapor

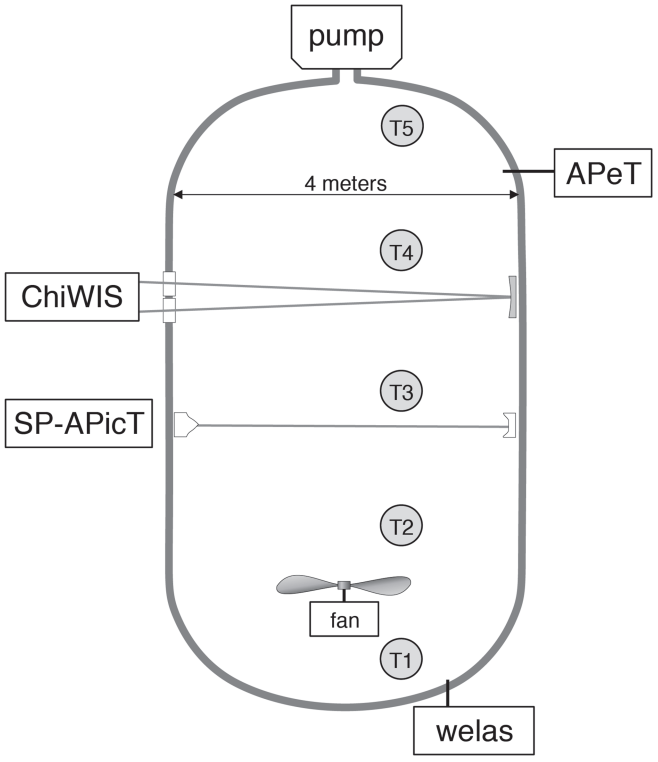

Fig. 1. Positioning of the instruments used in this analysis during the IsoCloud experiment campaigns. (Additional instruments also participated in the IsoCloud campaigns.) ChiWIS measures in situ isotopic water vapor (HDO/H_2O), SP-APicT [single-pass AIDA Physikalisch-Chemisches Institut (PCI) in cloud tunable diode laser (TDL)] measures in situ water vapor (H_2O only), and APeT (AIDA PCI extractive TDL) measures total water (H_2O ice and vapor). We take gas temperature as the average of thermocouples T1 through T4. Data from the welas optical particle counter are used to derive the effective ice particle diameter and in calculating kinetic isotope effects. SP-APicT data are used in cases of thick ice clouds to determine slight corrections for backscatter effects in ChiWIS.

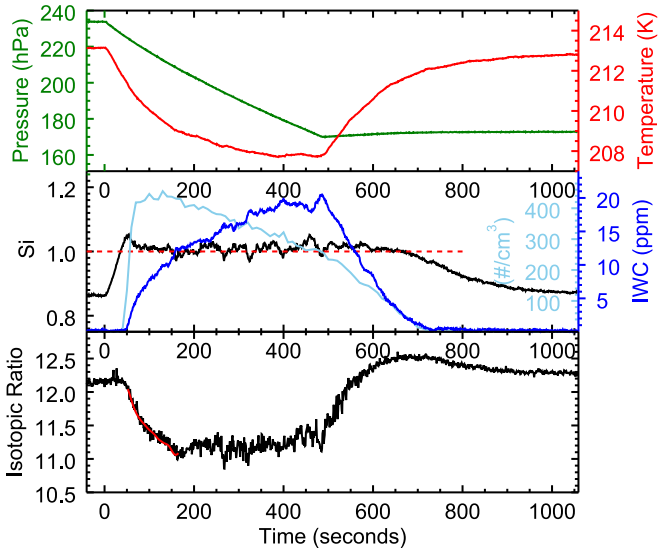

Fig. 2. Typical adiabatic expansion experiment. (*Top*) Pressure drop (green) causes drop in temperature (red) for ∼2 min before thermal flux from the wall becomes important. (*Center*) Ice formation [light blue, number density of ice particles; dark blue, total ice water content (IWC)] begins when critical supersaturation (black) is reached. (Ice water content is given in units of equivalent mixing ratio in chamber air—parts per million by volume—if ice were sublimated to the vapor phase.) (*Bottom*) Vapor isotopic ratio (black, doped to ∼12× natural abundance) shows three stages: initial decline as ice growth draws down vapor, constant period when ice growth is driven by wall flux, and final rise as ice sublimates. Fractionation factor is derived from model fit to initial period (red). After sublimation, vapor isotopic ratio exceeds starting value because of wall contribution; system then reequilibrates over ∼5 min. Fluctuations while ice is present reflect inhomogeneities due to turbulent mixing.

drops by 30 to 50% and the vapor HDO/H_2O ratio drops by ∼10%. After several minutes, the walls (prepared with a thin ice layer in initial isotopic equilibrium with vapor) become a source of both water vapor and heat (39), and vapor mixing ratio and isotopic composition stabilize even while ice growth continues. Most IsoCloud experiments reach saturation quickly after nucleation, but, in dilute conditions, ice growth can take several minutes to draw chamber vapor down to equilibrium. The resulting ambient supersaturation during ice growth depends on the nucleation threshold, growth rate, and ice particle number density.

The analysis here uses 28 experiments during the March through April 2013 IsoCloud campaign, covering a wide range of conditions: initial temperatures from 234 K to 194 K, mean supersaturation over ice (S_i) of 1.0 to 1.4, mean ice particle diameter of 2 μm to 14 μm, and ice nucleation via mineral dust, organic aerosols, and sulfate aerosols. (Temperatures are restricted to 234 K and below to preclude coexistence of liquid and ice phases, which would complicate isotopic interpretation.) Each campaign day involved four to six expansion experiments at the same initial temperature, separated by 1 h to 2 h to reestablish equilibrium. To boost signal to noise for isotopic measurements, all water introduced into AIDA was isotopically doped to produce HDO/H_2O ratios of ∼10 to 20× natural abundance (defined as VSMOW). See *SI Appendix* for further information about instruments, experiments, data treatment, and campaign. *SI Appendix*, Table S3 and Fig. S4 show conditions and results for all experiments used in this analysis.

Analysis

Interpreting cirrus formation experiments requires consideration of three factors: equilibrium fractionation, kinetic effects, and any additional sources of water. In the absence of other sources, water vapor isotopic composition would evolve by simple Rayleigh distillation, with vapor progressively depleted as ice grows and HDO is segregated into the ice phase. The effective isotopic fractionation $\alpha_{\mathrm{eff}} = \alpha_{\mathrm{eq}} \cdot \alpha_{\mathrm{k}}$ would then be the slope of that evolution (Fig. 3). Isotopic evolution deviates from Rayleigh distillation when the wall contribution becomes nonnegligible.

We account for all three effects by fitting each experiment to a model derived from mass balance over H_2O and HDO,

$$\frac{dR_v}{dt} = -\left(\alpha_{\mathrm{eff}} - 1\right) R_v \frac{P_{\mathrm{vi}}}{r_v} + \left(\gamma - 1\right) R_v \frac{S_{\mathrm{wv}}}{r_v}. \qquad [3]$$

(For further discussion, see *SI Appendix*, *Isotopic Model for Expansion Experiments*.) We measure the water vapor concentration r_v and isotopic composition $R_v = r'_v/r_v$ (where r'_v and r_v denote the mass mixing ratio of HDO and H_2O, respectively, in the vapor phase), and use water vapor and total water to infer P_{vi}, the loss of vapor to ice formation, and S_{wv}, the source of vapor from wall outgassing. The remaining two unknowns are the fractionation α_{eff} and $\gamma \equiv R_w/R_v$, the isotopic composition of wall flux ($R_w = r'_w/r_w$) normalized by that of bulk vapor.

We fit for these unknowns in two ways: fitting α_{eff} and γ independently (two-parameter fit) and assuming that outgassing is nonfractionating sublimation of ice that had previously equilibrated with chamber vapor, i.e., assuming $R_w = \alpha_{\mathrm{eq},0} \cdot R_{v0}$ (one-parameter fit). Results are consistent, suggesting that this assumption is valid. To minimize the influence of wall flux uncertainties, we fit only the initial part of each experiment when ice deposition dominates (54 s to 223 s): most ice growth occurs in the first few minutes of each experiment, and the wall contribution grows over time. See *SI Appendix*, *Fitting Protocol: Individual Experiments* for discussion of fitting individual experiments and uncertainty treatment.

To convert a derived effective fractionation α_{eff} into an equilibrium fractionation α_{eq}, we must assume a functional form for

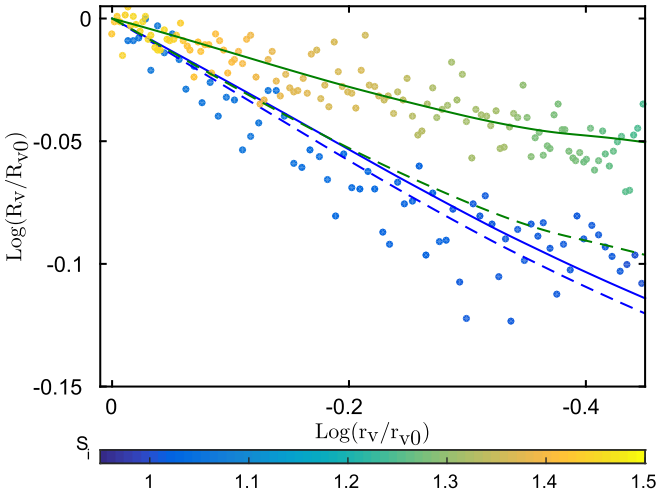

Fig. 3. Example illustrating reduced isotopic partitioning when ice grows in supersaturated conditions. Data points show 1-s measurements of R_v = [HDO]/[H_2O] in two expansion experiments (#27 and #45) at similar temperatures but with differing S_i (mean 1.01 and 1.35), plotted against evolving water mixing ratio r_v. Both axes are scaled to initial values because only relative changes are physically meaningful. The experiment proceeds from upper left to lower right, and the slope gives the effective fractionation $\alpha_{\mathrm{eff}} - 1$. Deviations from linearity result from changing S_i (and thus α_{k}), from changing temperature (and thus α_{eq}), and from wall flux. The two experiments show different effective fractionation (solid lines) but similar derived equilibrium fractionation (dashed lines).

α_k. We take as our default assumptions the classical model of Jouzel and Merlivat (27) (Eq. **2**) and isotopic diffusivity ratio d from Cappa et al. (30), but validate both assumptions using experiments in differing conditions of saturation and ice particle sizes. (See *Results* and *SI Appendix*, *Evaluation of Kinetic Models*.)

To derive the temperature dependence of the equilibrium fractionation factor, we first evaluate equilibrium fractionation factors for all 28 individual experiments, assuming evolving α_k from measured S_i and Eq. **2**. Because the experiments are performed at different temperatures, we can then estimate the temperature-dependent $\alpha_{eq}(T)$ by taking a weighted global fit of the 28 experimental α_{eq} values to the $1/T^2$ temperature dependence of Eq. **1**, constraining the fit to agree with the warmest measurement of Merlivat and Nief (22). (See *SI Appendix, Global Fit Procedure* for details; analysis implies that the functional form of Eq. **2** is indeed valid over this temperature range.)

Results

Equilibrium Fractionation Factor. We find that the temperature dependence of α_{eq} lies far below E13 (26), and slightly below the widely used M67 (22) (Fig. 4). The distinction from M67 (22) is significant to a 3σ confidence interval and robust to assumptions made in fitting and in modeling kinetic isotope effects. (The uncertainty estimates in Fig. 4 are used in weighting the global fit; see *SI Appendix, Fitting Protocol: Individual Experiments* for uncertainty, *SI Appendix, Fitting Protocol: Temperature Dependence* for global fitting, and *SI Appendix, Evaluation of Kinetic Models* for tests of kinetic models.) Estimates for $\alpha_{eq}(T)$ obtained by the two fitting methods differ by $< 10^{-2}$ throughout the experimental temperature range. We recommend that modelers use derived constants for the one-parameter fit: $a_0 = -0.0559$ and $a_1 = 13{,}525$; compare to M67 (22) with $a_0 = -0.0945$ and $a_1 = 16{,}289$.

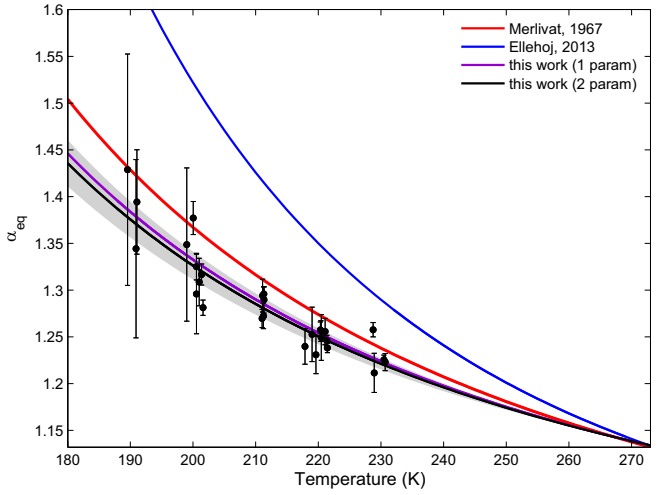

Fig. 4. Equilibrium vapor–ice fractionation factor for HDO/H_2O (α_{eq}) derived from 28 individual IsoCloud experiments. Black and purple lines show global fits through all experiments for two data treatments (black: one-parameter fit, wall flux composition R_w assumed to be that of ice initially at equilibrium with chamber vapor; purple: two-parameter fit, R_w as independent parameter). Dots show individual experiments (one-parameter), and gray shading shows the 3σ confidence interval on the global fit. Error bars represent 2σ uncertainties in fits to individual experiments. (These underestimate experimental error at warmer temperatures; see *SI Appendix, Fitting Protocol: Individual Experiments*.) Solid lines show M67 (ref. 22, red) and E13 (ref. 26, blue); these are derived from experiments at $T > 240$ K and 233 K, respectively. (See *SI Appendix*, Fig. S1 for experimental temperature ranges and all prior estimates of α_{eq}.) Results imply slightly weaker temperature dependence of α_{eq} than with M67 (22).

Kinetic Isotope Effects. As discussed previously, the inferred equilibrium fractionation values of Fig. 4 required correction for assumed kinetic modification, because any supersaturated conditions lead to lower effective isotopic fractionation (Fig. 3). The fact that IsoCloud experiments span a range of supersaturations allows us to quantitatively test models of kinetic isotope effects. Because equilibrium fractionation should depend only on temperature, a validity test for a kinetic model is that retrieved α_{eq} in individual experiments be independent of supersaturation: any dependence on S_i would imply an overcorrection or undercorrection for kinetic effects. We find that if α_k is estimated with the classic diffusive model of Eq. **2** and our default d = 1.0164 (30), the resulting fitted values for α_{eq} indeed show negligible dependence on supersaturation.

We can then extend this test to derive constraints on physical parameters in models of the kinetic effect. In each test case, we find the parameter value that yields a consistent α_{eq} independent of S_i, along with 1σ bounds from propagation of uncertainties. (See *SI Appendix*, *Evaluation of Kinetic Models* for details.) Estimating the isotopic diffusivity ratio d under the pure diffusive model of Eq. **2** yields an optimal value slightly below the lowest published measurement, although with uncertainty encompassing all literature values (Fig. 5). The optimized value is 1.009 ± 0.036, whereas published estimates of d evaluated at 190 K span 1.015 to 1.045 (*SI Appendix*, Table S5). Although this constraint is not strong, it motivates our choice of the relatively low diffusivity ratio measured by Cappa et al. (30) as our default, a value that is also consistent with kinetic gas theory.

We next test a model that incorporates surface kinetic effects following Nelson (29) (*SI Appendix*, Fig. S10). In this model, the isotopic diffusivity ratio d in Eq. **2** is replaced by $(\mathrm{d}k + \mathrm{xy})/(1 + k)$, where x is the ratio of deposition coefficients, y is the ratio of thermal velocities ($\sqrt{19/18}$), and the dimensionless coefficient $k \equiv rv\beta/4D_v$, where r is the ice particle radius and v, D_v, and β are the thermal velocity, diffusivity in air, and deposition coefficient for H_2O, respectively. Note that this surface kinetic model does not reduce to the pure diffusive model of Eq. **2** when x is set to 1 but, when fit to the experiments described here, produces nearly identical results. The limited IsoCloud experiments do not allow d and x to be constrained simultaneously, but we can estimate each given an assumption about the other. We therefore optimize for x in the surface kinetic model given a variety of assumed d.

These tests yield x slightly below 1 regardless of the assumed diffusivity ratio. At the low default d = 1.0164, we obtain $\mathrm{x} = 0.957 \pm 0.22$ (*SI Appendix*, Fig. S10). The higher the assumed value of d, the lower the implied value of x; for example, d = 1.0251 (40) yields x = 0.924 (again $\pm$ 0.22). These experiments may therefore provide tighter constraints on x than the range of 0.8 to 1.2 suggested by Nelson (29). The results consistently suggest that HDO molecules are slightly more likely to be incorporated into the crystal lattice than are H_2O.

Discussion

Given the extensive use of water isotopic variations in climate, atmospheric, and planetary studies, the paucity of measurements of the fundamental fractionation properties of water has long been a concern. This concern was heightened by the recent significant proposed revision by Ellehøj et al. (26) to the half-century-old measurements of Merlivat and Nief (22). The experiments described here should provide some resolution of that discrepancy. The IsoCloud campaign allowed direct measurements of the equilibrium fractionation factor between HDO and H_2O at the cold temperatures characteristic of cirrus clouds, polar snow, or Martian snow and ice deposits. These measurements rule out the substantial upward revision to α_{eq} proposed by Ellehøj et al. (26) and, in fact, imply a slightly weaker temperature

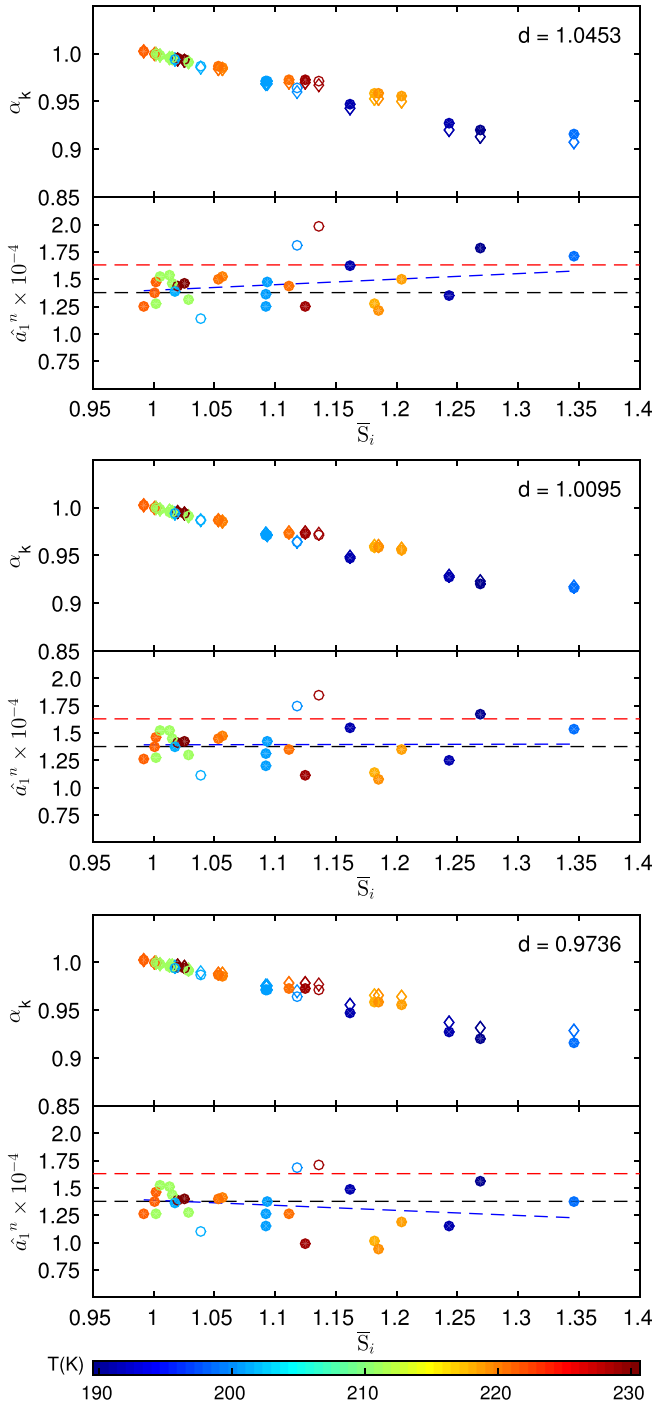

Fig. 5. Effect of choice of d (ratio of isotopic diffusivities) on calculated kinetic effects and retrieved equilibrium fractionation in experiments, plotted against deposition-weighted supersaturation. Top halves of panels show kinetic factors for different experiments using the diffusive model of Jouzel and Merlivat (27) and the stated value of d (circles), and, for reference, identical calculations using the default d = 1.0164 (open diamonds). Bottom halves show resulting equilibrium fractionations, for each experiment, as the a_1 parameters estimated in fitting each experiment n to Eq. **1**, assuming the same constraint as in the global fit. (See *SI Appendix, Tests of Kinetic Models* and Fig. S9.) Deviation from slope 0 implies a misspecified kinetic model. Dashed lines show a_1 values corresponding to M67 (ref. 22, red) and this work (black). Blue line is weighted fit to $\hat{a}_1^n$, excluding three outlier experiments (#4, #26, and #48, shown as open circles). The three panels show the fitted optimal value for d and conservative upper and lower bounds. Bounds span the range of published estimates of d. (See *SI Appendix*, Fig. S10 for similar analysis on x, the ratio of isotopic deposition coefficients.)

dependence and therefore slightly lower equilibrium fractionation than that of Merlivat and Nief (22).

The IsoCloud campaign also provided quantitative confirmation of theories of the kinetic modification to fractionation during ice deposition. Cirrus formation experiments in supersaturated conditions demonstrate that the diffusive model for kinetic isotope effects originally proposed 3 decades ago provides an adequate explanation of suppressed fractionation when ice growth is diffusion-limited. Experiments show slightly weaker kinetic effects than expected with the perhaps most widely used estimate of the isotopic diffusivity ratio (d = 1.0251 from ref. 40) but are consistent with the slightly lower estimate of Cappa et al. (d = 1.0164) (30).

Experimental results are also consistent with a surface kinetic model that posits additional modifications to fractionation due to isotopic differences in incorporation into the ice lattice. Fits to this model consistently suggest a slightly higher deposition coefficient for HDO than for H_2O, although the results cannot exclude equal values. However, the limited set of IsoCloud experiments allows for multiple solutions: an even stronger surface effect favoring HDO deposition could be counteracted by an even stronger diffusion effect preferentially bringing H_2O to the growing ice particle.

The constraints on diffusivity and deposition ratios obtained here could be tightened further given a targeted series of experiments. In IsoCloud, the experiments with conditions most sensitive to kinetic effects tended to be those at the coldest temperatures, where signal-to-noise is lowest. Diffusion-related effects play a role only in supersaturated conditions; in the IsoCloud experiments, homogeneous nucleation experiments with high S_i were conducted only at $T < 205$ K. Surface effects play a role only when k and therefore ice crystal size are small; in IsoCloud, these conditions again occurred only at the coldest temperatures. Values for k (2 to 15) followed ice particle diameters (2 μm to 14 μm), which followed temperature; in IsoCloud, diameters below 5 μm dominated only for $T < 215$ K. New experiments at warmer (> 220 K) temperatures that systematically varied ice crystal diameters in high-supersaturation conditions could allow distinguishing diffusion from surface effects.

Note that, although these methods can, in principle, be used to evaluate fractionation in other isotopologues of water, the oxygen-substituted isotopic systems are more challenging because of their smaller vapor pressure isotope effects: at 190 K, $\alpha_{eq} < 1.04$ for $H_2^{18}O/H_2O$ vs. 1.4 for HDO/H_2O (41). Isotopic doping is, however, particularly useful for the low-natural-abundance $H_2^{17}O$.

Although the particular set of IsoCloud experiments provides only broad constraints on kinetic isotope effects, they demonstrate the potential of in situ vapor measurements in dynamic condensation experiments for diagnosing fundamental isotope physics. All previous approaches to determining equilibrium and kinetic isotopic fractionation in water relied on setting up static conditions and measuring differences or gradients in space. We demonstrate here the power of measuring, instead, evolution over time, in conditions more analogous to condensation in real naturally occurring systems. IsoCloud results show that chamber-based simulations of ice growth in cirrus clouds can provide robust estimates of equilibrium fractionation in the vapor–ice system, and robust constraints on kinetic effects. We hope this approach helps enable further measurements of the fundamental isotopic properties of water and other condensable species.

ACKNOWLEDGMENTS. The many IsoCloud participants contributed greatly to the success of the campaign, including Stephanie Aho, Jan Habig, Naruki Hiranuma, Erik Kerstel, Benjamin Kühnreich, Janek Landsberg, Eric Stutz, Steven Wagner, and the AIDA technical staff and support team. Marc Blanchard provided data from Pinilla et al., 2014 (42) for the comparison of *SI Appendix*, Fig. S1. We thank Thomas Ackerman, Marc Blanchard, Peter Blossey, Won Chang, Albert Colman, Nicolas Dauphas, John Eiler,

Edwin Kite, and William Leeds for helpful discussions and comments. Funding for this work was provided by the National Science Foundation (NSF) and the Deutsche Forschungsgemeinschaft through International Collaboration in Chemistry Grant CHEM1026830. K.D.L. acknowledges support from a National Defense Science and Engineering Graduate Fellowship and an NSF Graduate Research Fellowship, and L.S. acknowledges support from a Camille and Henry Dreyfus Postdoctoral Fellowship in Environmental Chemistry.

1. Jouzel J, Koster RD (1996) A reconsideration of the initial conditions used for stable water isotope models. *J Geophys Res Atmos* 101:22933–22938.
2. Bony S, Risi C, Vimeux F (2008) Influence of convective processes on the isotopic composition (δ^{18}O and δD) of precipitation and water vapor in the tropics: 1. Radiative-convective equilibrium and Tropical Ocean-Global Atmosphere-Coupled Ocean-Atmosphere Response Experiment (TOGA-COARE) simulations. *J Geophys Res Atmos* 113:D19305.
3. Gedzelman SD, Arnold R (1994) Modeling the isotopic composition of precipitation. *J Geophys Res Atmos* 99:10455–10471.
4. Risi C, Bony S, Vimeux F (2008) Influence of convective processes on the isotopic composition (δ^{18}O and δD) of precipitation and water vapor in the tropics: 2. Physical interpretation of the amount effect. *J Geophys Res Atmos*113:D19306.
5. Moyer EJ, Irion FW, Yung YL, Gunson MR (1996) ATMOS stratospheric deuterated water and implications for troposphere-stratosphere transport. *Geophys Res Lett* 23:2385–2388.
6. Hanisco TF, et al. (2007) Observations of deep convective influence on stratospheric water vapor and its isotopic composition. *Geophys Res Lett* 34:L04814.
7. Randel WJ, et al. (2012) Global variations of HDO and HDO/H_2O ratios in the upper troposphere and lower stratosphere derived from ACE-FTS satellite measurements. *J Geophys Res Atmos* 117:D06303.
8. Blossey PN, Kuang Z, Romps DM (2010) Isotopic composition of water in the tropical tropopause layer in cloud-resolving simulations of an idealized tropical circulation. *J Geophys Res Atmos* 115:D24309.
9. Bolot M, Legras B, Moyer EJ (2013) Modelling and interpreting the isotopic composition of water vapour in convective updrafts. *Atmos Chem Phys* 13:7903–7935.
10. Montmessin F, Fouchet T, Forget F (2005) Modeling the annual cycle of HDO in the Martian atmosphere. *J Geophys Res Planets* 110:E03006.
11. Villanueva G, et al. (2015) Strong water isotopic anomalies in the Martian atmosphere: Probing current and ancient reservoirs. *Science* 348:218–221.
12. Sayres DS, et al. (2010) Influence of convection on the water isotopic composition of the tropical tropopause layer and tropical stratosphere. *J Geophys Res Atmos* 115:D00J20.
13. Herbin H, Coheur PF, Hurtmans D, Clerbaux C (2007) Tropospheric water vapour isotopologues ($H_2^{16}O$, $H_2^{18}O$, $H_2^{17}O$ and HDO) retrieved from IASI/METOP data. *Atmos Chem Phys* 7:3957–3968.
14. Worden J, et al. (2012) Profiles of CH_4, HDO, H_2O, and N_2O with improved lower tropospheric vertical resolution from Aura TES radiances. *Atmos Meas Tech* 5:397–411.
15. Nassar R, et al. (2007) Variability in HDO/H_2O abundance ratios in the tropical tropopause layer. *J Geophys Res Atmos* 112:D21305.
16. Steinwagner J, et al. (2007) HDO measurements with MIPAS. *Atmos Chem Phys* 7:2601–2615.
17. Urban J, et al. (2007) Global observations of middle atmospheric water vapour by the Odin satellite: An overview. *Planet Space Sci* 55:1093–1102.
18. Vandaele A, et al. (2011) NOMAD, a spectrometer suite for nadir and solar occultation observations on the ExoMars Trace Gas Orbiter. *Mars Atmosphere: Modelling and Observation*, eds Forget F, Millour M (Lab Metereol Dyn, Paris), pp 484–487.
19. Joussaume S, Sadourny R, Jouzel J (1984) A general circulation model of water isotope cycles in the atmosphere. *Nature* 311:24–29.
20. Jouzel J, et al. (1987) Simulations of the HDO and $H_2^{18}O$ atmospheric cycles using the NASA GISS general circulation model: The seasonal cycle for present-day conditions. *J Geophys Res Atmos* 92:14739–14760.
21. Lee JE, Fung I, DePaolo DJ, Henning CC (2007) Analysis of the global distribution of water isotopes using the NCAR atmospheric general circulation model. *J Geophys Res Atmos* 112:D16306.
22. Merlivat L, Nief G (1967) Fractionnement isotopique lors des changements d'état solide-vapeur et liquide-vapeur de l'eau à des températures inférieures à 0°C. *Tellus* 19:122–127.
23. Criss RE (1991) Temperature dependence of isotopic fractionation factors. *Stable Isotope Geochemistry: A Tribute to Samuel Epstein*, eds Taylor HP, O'Neil JR, Kaplan IR (Geochem Soc, Washington, DC), Vol 3, pp 11–16.
24. Dauphas N, Schauble E (2016) Mass fractionation laws, mass-independent effects, and isotopic anomalies. *Annu Rev Earth Planet Sci* 44:709–783.
25. Bigeleisen J, Mayer M (1947) Calculation of equilibrium constants for isotopic exchange reactions. *J Chem Phys* 15:261–267.
26. Ellehøj MD, Steen-Larsen HC, Johnsen SJ, Madsen MB (2013) Ice-vapor equilibrium fractionation factor of hydrogen and oxygen isotopes: Experimental investigations and implications for stable water isotope studies. *Rapid Commun Mass Spectrom* 27:2149–2158.
27. Jouzel J, Merlivat L (1984) Deuterium and oxygen 18 in precipitation: Modeling of the isotopic effects during snow formation. *J Geophys Res* 89:11749–11757.
28. Dansgaard W (1964) Stable isotopes in precipitation. *Tellus* 16:436–468.
29. Nelson J (2011) Theory of isotopic fractionation on facetted ice crystals. *Atmos Chem Phys* 11:11351–11360.
30. Cappa CD, Hendricks MB, DePaolo DJ, Cohen RC (2003) Isotopic fractionation of water during evaporation. *J Geophys Res Atmos* 108:11351.
31. Uemura R, Matsui Y, Yoshida N, Abe O, Mochizuki S (2005) Isotopic fractionation of water during snow formation: Experimental evidence of kinetic effect. *Polar Meteorol Glaciol* 19:1–14.
32. Casado M, et al. (2016) Experimental determination and theoretical framework of kinetic fractionation at the water vapour-ice interface at low temperature. *Geochim Cosmochim Acta* 174:54–69.
33. DePaolo D (2011) Surface kinetic model for isotopic and trace element fractionation during precipitation of calcite from aqueous solutions. *Geochim Cosmochim Acta* 75:1039–1056.
34. Takahashi T, Endoh T, Wakahama G, Fukuta N (1991) Vapor diffusional growth of free-falling snow crystals between -3 and -23°C. *J Meteorol Soc Jpn Ser* 69:15–30.
35. Nelson J (2005) Branch growth and sidebranching in snow crystals. *Crystal Growth Design* 5:1509–1525.
36. Möhler O, et al. (2003) Experimental investigation of homogeneous freezing of sulphuric acid particles in the aerosol chamber aida. *Atmos Chem Phys* 3:211–223.
37. Möhler O, et al. (2006) Efficiency of the deposition of mode ice nucleation on mineral dust particles. *Atmos Chem Phys* 6:3007–3021.
38. Cziczo D, et al. (2013) Ice nucleation by surrogates of Martian mineral dust: What can we learn about Mars without leaving Earth? *J Geophys Res Planets* 118:1945–1954.
39. Cotton RJ, Benz S, Field P, Möhler O, Schnaiter M (2007) Technical note: A numerical test-bed for detailed ice nucleation studies in the aida cloud simulation chamber. *Atmos Chem Phys* 7:243–256.
40. Merlivat L (1978) Molecular diffusivities of $H_2^{16}O$, $HD^{16}O$, and $H_2^{18}O$ in gases. *J Chem Phys* 69:2864–2871.
41. Majoube M (1971) Fractionation in O-18 between ice and water vapor. *J Chim Phys Phys Chim Biol* 68:625–636.
42. Pinilla C, et al. (2014) Equilibrium fractionation of H and O isotopes in water from path integral molecular dynamics. *Geochemica et Cosmochemica Acta* 135:203–216.